CERN-LPCC-2017-XX

Dark Matter Working Group recommendation for Two Higgs Doublet Model (draft title)

Authorlist to be compiled; Antonio Boveia,[3,*] Caterina Doglioni,[8,*] Kristian Hahn,[14,*] Ulrich Haisch,[15,16,*] Steven Lowette,[22] Tim M.P. Tait,[25,*]

[*]DMWG organizers

[3]Ohio State University, 191 W. Woodruff Avenue Columbus, OH 43210

[8]Fysiska institutionen, Lunds universitet, Lund, Sweden

[14]Department of Physics and Astronomy, Northwestern University, Evanston, Illinois 60208, USA

[15]Rudolf Peierls Centre for Theoretical Physics, University of Oxford, Oxford, OX1 3PN, United Kingdom

[16]CERN, TH Department, CH-1211 Geneva 23, Switzerland

[22]Physics Department, Vrije Universieit Brussel, Brussels, Belgium

[25]Department of Physics and Astronomy, University of California, Irvine, California 92697, USA

Editor's E-mail: antonio.boveia@cern.ch, caterina.doglioni@cern.ch, kristian.hahn@cern.ch, ulrich.haisch@physics.ox.ac.uk, ttait@uci.edu

Abstract. Draft abstract.

Contents

1 Model kinematics and mapping to existing models

The signature and kinematic distributions of the 2HDM+a model at colliders are determined by the values assigned to the parameters described in the previous chapter. The model parameters can affect the total signal cross-section, the kinematic distributions, or both. In order to obtain a representative grid of benchmark points for collider searches and reduce this multi-dimensional parameter space, we scan ranges of the possible values of these parameters and observe the impact on the kinematic distributions for representative collider searches.

In this chapter, we will outline the existing experimental searches that can be used to search for this model, and present the distributions of the kinematic variables for each of the searches as a function of the free parameters of the model. We note that in the following we have chosen to fix the DM coupling y_χ to unity, and $\lambda_{P1} = \lambda_{P2} = \lambda_P = 3$ as explained in **??**.

1.1 Description of experimental searches

1.1.1 Signatures including a Higgs boson

$h(bb) + E_T^{\text{miss}}$ signature The results from this search are at parton level, based on the model-independent results in [1].

1.1.2 Signatures including a Z boson

Events with a Z boson and E_T^{miss} may signal the presence of invisible particles recoiling against the Z boson [2, 3]. LHC searches (e.g. [4, 5] for the most recent ones) have focused on invisible decays of the SM-like Higgs bosons or on topologies where the Z boson is produced as initial-state radiation (ISR) from a quark. The ISR-based topologies generically

favor radiation of a gluon or photon rather than a massive gauge boson, thus limiting the discovery sensitivity of a Z-based approach compared to monojet and mono-photon searches. In contrast, the model studied in this document generates the mono-Z signature dominantly via the all-bosonic H-a-Z vertex, which can lead to enhancements in the mono-Z sensitivity compared to jet and photon signatures.

Mono-Z (leptonic) signature Three consecutive stages of event selection are considered in the case the Z decays leptonically:

- Inclusive: Lepton p_T and η requirements corresponding to the typical experimental trigger acceptance are applied.
- Preselection: A dilepton candidate with an invariant mass in a window around the Z mass is required, and a minimum transverse momentum of the $\chi\overline{\chi}$ system is required.
- Final selection: Requirements on the main discriminating variables used in the relevant analyses are added: The angular separation in the transverse plane between the $\chi\overline{\chi}$ and $l^+\,l^-$ systems $\Delta\Phi(ll, E_T^{\text{miss}})$, the relative transverse momentum difference between them $|p_{T,ll} - E_T^{\text{miss}}|/p_{T,ll}$ and the angular separation between the leptons $\Delta R(ll)$. Additionally, the E_T^{miss} requirement is tightened.

The exact event selection criteria are listed in the appendix, in **??**. The results in this and in the following section are at particle level.

Mono-Z (hadronic) signature The hadronic signature in Z+E_T^{miss} events ($Z \to q\bar{q}$ decays in association with large missing transverse momentum) is complementary to the leptonic signature. Hadronic decays are more frequent than leptonic decays, but suffer from larger backgrounds. For these reasons, the Z (hadronic) + E_T^{miss} search is favored if the model include higher mass scalar and pseudoscalar bosons.

The event selection in this case changes depending on the production transverse momentum of the Z-boson, as in the case of the exchange of a high-mass CP-even H boson. If the Z-boson is boosted, then its hadronic decay products could be merged into a single jet, and the Z to QCD background discrimination can be improved by exploiting the presence of substructure within a single, large-radius jet (denoted by J). The *boosted* search is performed in addition to the *resolved* search, where the Z decay products are reconstructed as two separate small-radius jets (denoted by j).

For mono-$Z(\to q\bar{q})$ events intermediated by the exchange of a high-mass CP-even H boson, the Z-boson will be produced with a large transverse momentum and the hadronic decay products of such Z-boson could be merged into a single jet. Such "boosted" event topology is investigated by exploiting the reconstruction technique with a large-radius jet (denoted by J), in addition to more conventional "resolved" event topology where the Z decay products are reconstructed as two separate small-radius jets (denoted by j). The jet reconstruction and the following analysis are all performed at particle level after showering and hadronization implemented in Pythia 8.212 described above.

Two consecutive stages of event selection are considered for the boosted and resolved event topologies:

- Inclusive: minimal kinematic requirements are applied to a pair of small-radius jets (a single large-radius jet) for the resolved (boosted) event topology. These selection criteria are applied separately, i.e, not sequentially.

- Final selection: selection criteria are applied to the a number of variables. The invariant mass of the pair of small-radius jets or the single large-radius jet is required to be within a window around the Z mass. In addition, selection is applied to the azimuthal angular difference between the $\chi\overline{\chi}$ and the hadronic Z-boson system, $\Delta\Phi(jj \text{ or } J, E_T^{\text{miss}})$, and the magnitude of E_T^{miss}. These final selection cuts are applied sequentially to mimic a realistic analysis; in this study the boosted selection cuts are applied first and then the resolved selection cuts are applied to those events that fail the boosted ones.

The exact event selection criteria are listed in the appendix, in **??**. The results in this and in the following section are at particle level.

1.1.3 Signatures including heavy flavor quarks

Heavy flavor final state can have sizable contributions to the production of the CP-even and CP-odd scalar mass eigenstates, due to the Yukawa structure of the couplings in the SM sector.

1.2 Kinematic distributions justifying the choice of parameter scan

1.2.1 Masses of the A and a, $H^{\pm}$ and H bosons (M_A, M_a, $M_{H^{\pm}}$ and M_H)

The **masses M_A and M_a of the pseudoscalars A and a**, which represent the two mediators in **??**, affect the shape of the E_T^{miss} distribution

In the mono-Z and mono-H channels, the main production process is from the $2 \to 1 \to 2$ processes $gg \to A \to ah$, and $gg \to H \to aZ$, respectively, with the light pseudoscalar decaying invisibly as $a \to \chi\chi$. In this case, the $A/H \to ah$ process produces a resonance in the invariant mass distribution of the final state system with a width determined by the widths of a, A/H, and of the SM bosons. This results in a peak in the transverse momentum distribution of the DM system, reconstructed as E_T^{miss} in the detector.

The location of this Jacobian peak can be calculated analytically starting from the masses of the particles involved in the decay [6]:

$$E_T^{\text{miss},max} \approx \frac{\sqrt{\left(M_{A/H}^2 - M_a^2 - M_{h/Z}^2\right)^2 - 4M_a^2 M_{h/Z}^2}}{2M_{A/H}}. \tag{1.1}$$

Thus, increasing M_A results in a Jacobian peak at higher E_T^{miss}, as shown in Figure 1a, Figure 2 and Figure 3. Conversely, models with higher M_a have a Jacobian peak at lower E_T^{miss}, as indicated in Figure 1b and Figure 4. For $M_{A/H} \approx M_a + m_{Z/h}$, both the a and Z/h bosons are produced approximately at rest, leading to an event population with overall low boost. These qualitative trends are consistent with the distributions of the other main selection variables as shown in the appendix (**??**).

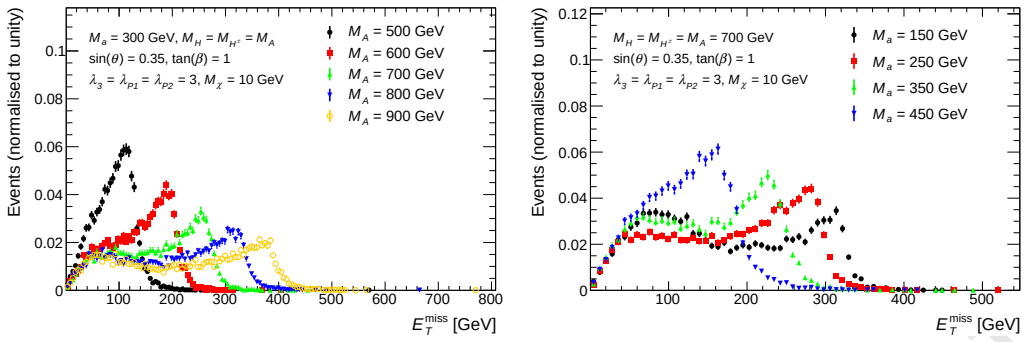

(a) E_T^{miss} distribution for points with different M_A ($= M_H = M_{H^\pm}$) and fixed $M_a = 300$ GeV.

(b) E_T^{miss} distribution for points with different M_a and fixed $M_A = M_H = M_{H^\pm} = 700$ GeV.

Figure 1: Parton-level E_T^{miss} distribution in $h(bb) + E_T^{\text{miss}}$ events for different M_a and M_A, with $\sin\theta = 0.35, \tan\beta = 1, M_\chi = 10$ GeV and $\lambda_{P1} = \lambda_{P2} = \lambda_3 = 3$

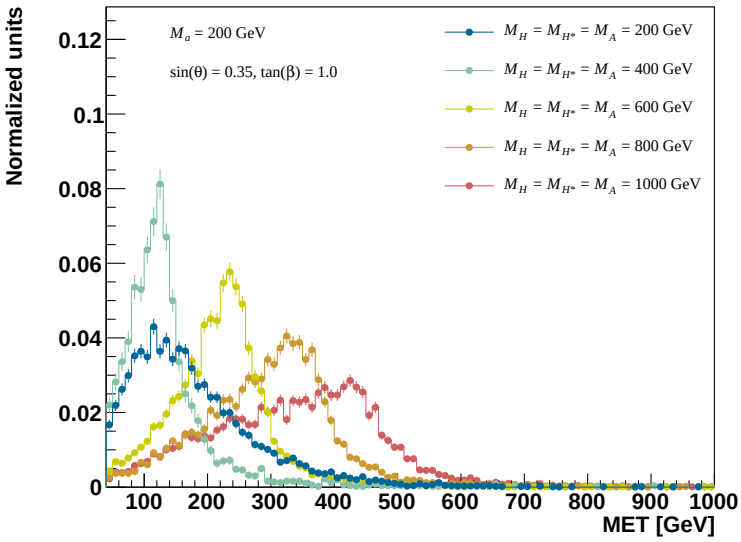

Figure 2: The E_T^{miss} distribution in signatures including a Z boson after preselection in the leptonic channel, with varying M_A values for fixed $M_a = 200$ GeV and $M_A = M_H$.

A fraction of the signal events is also produced in non-resonant $2 \to 3$ processes $gg \to h\chi\chi$, as in **??**, leading to a broader distribution of the invariant mass of the decay products. Consequently, this results in a broader and softer E_T^{miss} distribution that is distinct from the Jacobian peak discussed above, and contributes to the off-peak features of Figure 1b and Figure 1a.

The masses M_a and M_A influence the kinematics in the $t\bar{t} + E_T^{\text{miss}}$ signature as well. As shown in Figure 5, the E_T^{miss}, and leading and trailing top quark p_T distributions broaden with increasing M_a. Similarly, for values of $M_A < M_a$, as M_A increases, the

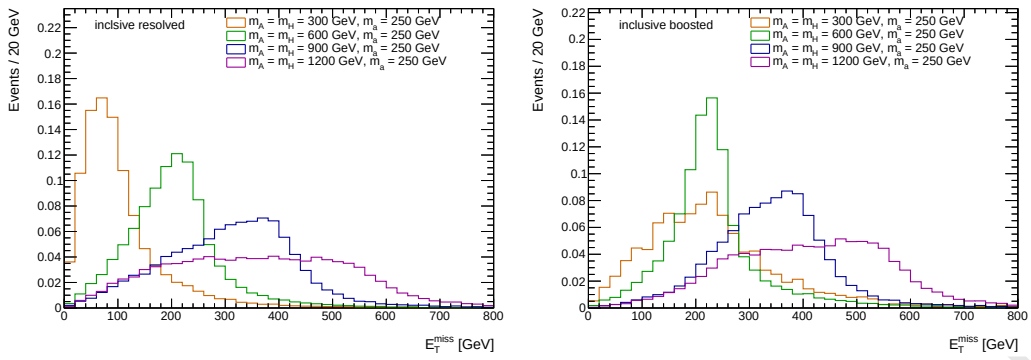

Figure 3: E_T^{miss} distributions in the resolved (left) and boosted (right) hadronic Z search, after applying the inclusive selection. The signal masses are chosen to be M_A = 300, 600, 900 and 1200 GeV with the fixed M_a = 250 GeV.

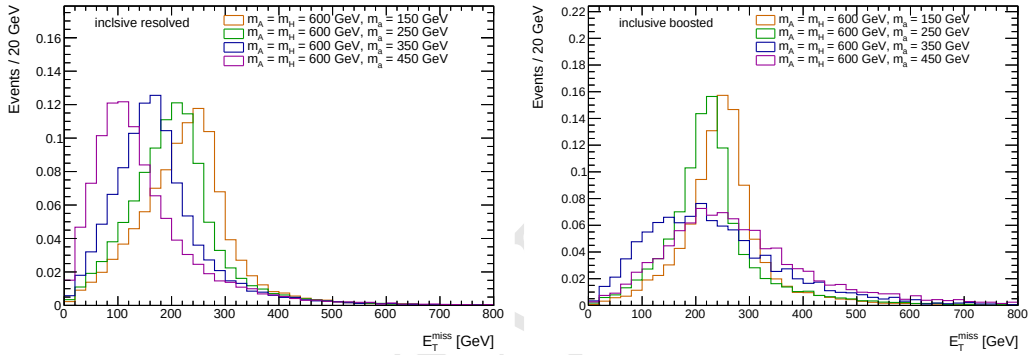

Figure 4: E_T^{miss} distributions in the resolved (left) and boosted (right) hadronic Z search, after applying the inclusive selection. The signal masses are chosen to be M_a = 150, 250, 350 and 450 GeV with the fixed M_A = 600 GeV.

kinematic distributions mentioned above also broaden, as shown in Figure 6.

Since the shape of the E_T^{miss} distribution affects the design of experimental searches, and to a large extent their sensitivity, *it is desirable to scan the M_A and M_a parameter space.*

In designing a search for evidence of this particular model, it may be useful to consider not only the E_T^{miss}, but also the transverse mass M_T[1] variable. The distributions of both variables after final selection are shown in Figure 7 for the Z+E_T^{miss} searches. Both distributions show Jacobian peak structures due to dominant effect of the diagram with resonant H exchange. In the case of $M_a < M_H$, the peak structure is more defined in the M_T distribution than in the E_T^{miss}, thus helping to distinguish a possible signal from background. Where the resonant diagram does not contribute, i.e. for $M_a \approx M_H$ or $M_a > M_H$, the M_T distribution does not show a significantly different structure from the E_T^{miss} distribution and will not provide an improved sensitivity.

[1]The massless definition is used here: $M_T = \sqrt{2E_T^{\text{miss}} p_{\text{T,Z}} (1 - \cos(\Delta\phi))}$

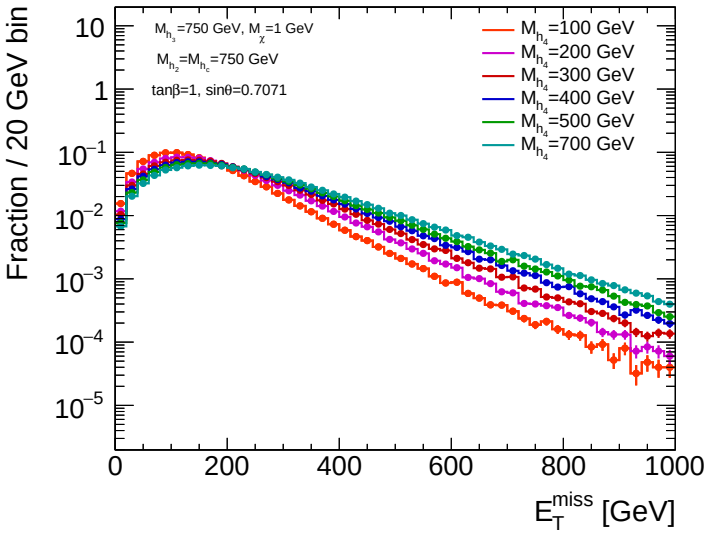

(a) E_T^{miss}

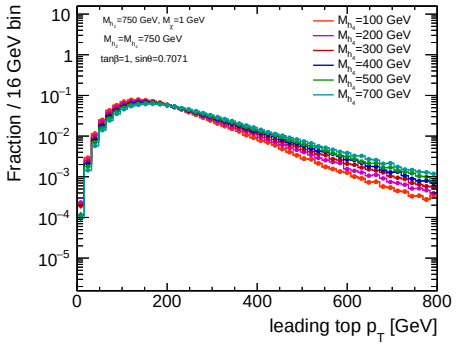

(b) Leading top quark p_T

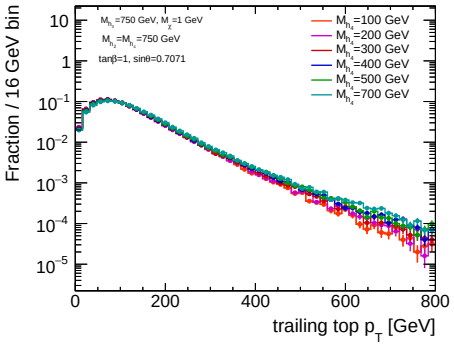

(c) Trailing top quark p_T

Figure 5: The E_T^{miss}, leading and trailing top p_T distributions for inclusive $t\bar{t} + \chi\bar{\chi}$ production for various values of M_a, with $M_A = 750$ GeV, $M_H = M_{H^\pm} = 750$ GeV, $\tan\beta = 1$, and $\sin\theta = 0.7071$.

The **mass of the heavy neutral scalar Higgs boson** H has an indirect effect on the rate and kinematics of the signal. This is caused by the dependence of the coupling strengths and thus decay widths of the pseudoscalars A and a on M_H [6]. Therefore, a change of M_H can affect the relative contribution of resonant versus non-resonant signal processes, as illustrated in Figure 8.

The choice $M_H = M_A$ results in a detectable total cross section for many signal points and a dominant contribution of the resonant signal process. This choice allows us to test diverse E_T^{miss} distributions and results in about equal contributions to the sensitivity through the $Z + E_T^{\text{miss}}$ and $h + E_T^{\text{miss}}$ signatures, highlighting their complementarity. For this reason *the choice* $M_H = M_A$ *is adopted* for all scans.

The mass of the neutral scalar $H^\pm$ does not affect the model kinematics, as shown

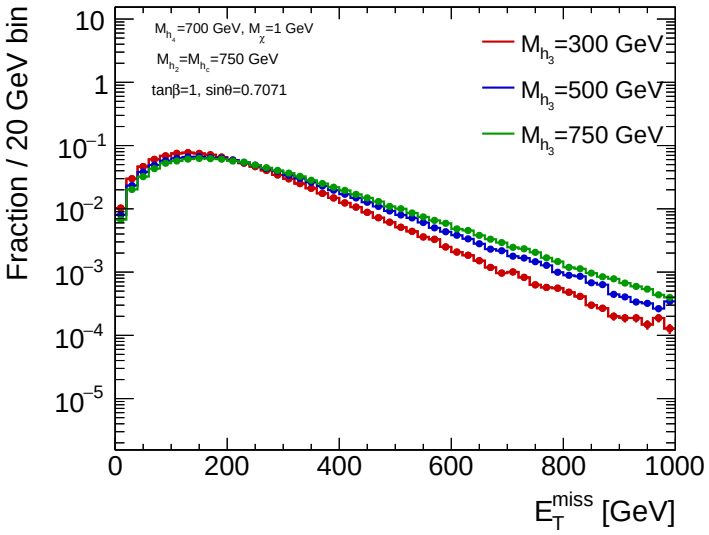

(a) E_T^{miss}

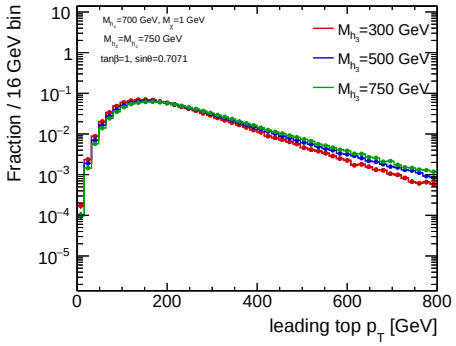

(b) Leading top p_T

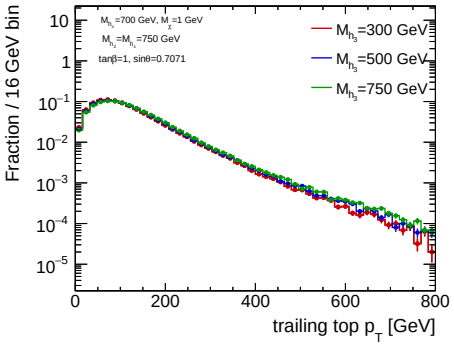

(c) Trailing top p_T

Figure 6: The E_T^{miss}, leading and trailing top p_T distributions for inclusive $t\bar{t} + \chi\bar{\chi}$ production for various values of M_A, with M_a = 700 GeV, M_H = $M_{H^\pm}$ = 750 GeV, $\tan\beta = 1$, and $\sin\theta = 0.7071$, before any analysis selection.

in Appendix **??**. Therefore, for simplicity, the *neutral scalar* $H^\pm$ *is assumed to be mass-degenerate to* H.

1.2.2 Mixing angle between the two pseudoscalars A and a ($\sin\theta$)

The sine of the mixing angle between the two pseudoscalars A and a, $\sin\theta$, affects not only the cross section, but also the shape of the E_T^{miss} distribution in searches including a Higgs boson, as shown in Figure 12a. For the resonant diagram $gg \to A \to ah \to \chi\bar{\chi}h$, the product of cross section times branching ratios $\mathcal{B}(A \to ah)\mathcal{B}(a \to \chi\bar{\chi})$ scales with $\sin^2\theta\cos^6\theta$, while for the diagram $gg \to a \to A^*h \to \chi\bar{\chi}h$, the product of cross section times branching ratios $\mathcal{B}(a \to Ah)\mathcal{B}(A \to \chi\bar{\chi})$ scales with $\sin^6\theta\cos^2\theta$. This is shown in Appendix **??**. Therefore, at small $\sin\theta$, the resonant diagram $A \to ah$ is the dominant

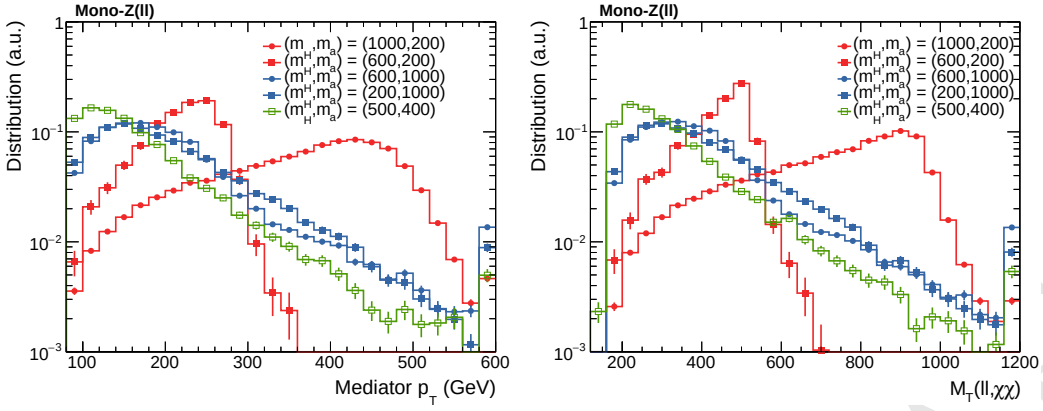

Figure 7: E_T^{miss} and M_T distributions after the full selection of Z(lep)+E_T^{miss} search. Both distributions show a peaked structure around M_H in the $M_H > M_a$ regime, reflecting the resonant production of H with a subsequent decay $H \to aZ$.

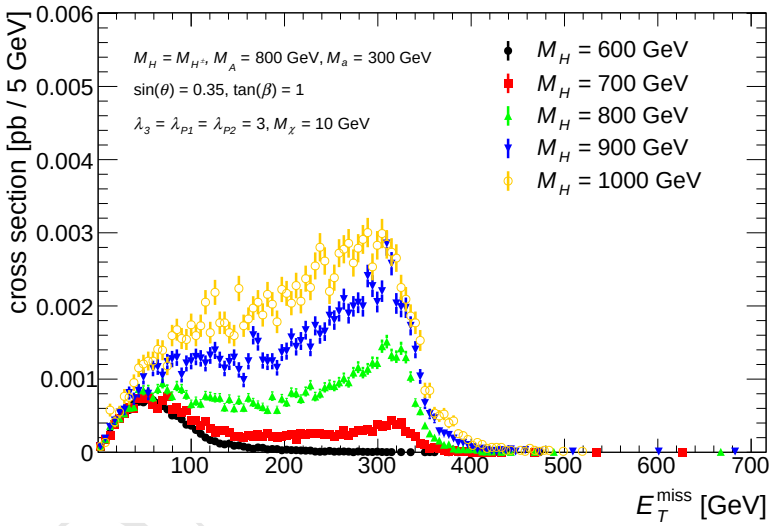

Figure 8: The E_T^{miss} distribution, accounting for the production cross section, of $h(bb) + E_T^{\text{miss}}$ signal events for five representative choices of $M_H = M_{H^\pm}$.

Figure 9: E_T^{miss} distribution in $h(bb) + E_T^{\text{miss}}$ and Z+E_T^{miss} events for different M_H

production mode and the E_T^{miss} distribution has a Jacobian peak following Equation 1.1; while at large $\sin\theta$, the $a \to A^*h$ diagram starts to dominate and produces a second peak at a lower E_T^{miss} value.

In the $h(bb) + E_T^{\text{miss}}$ case, the shape of the E_T^{miss} distribution does not change much for $\sin\theta < 0.7$, then changes significantly for $\sin\theta \geq 0.7$. When $\sin\theta = 0.9$, the diagram $gg \to a \to A^*h \to \chi\bar{\chi}h$, producing a E_T^{miss} peak at around 60 GeV, starts to dominate. Following these studies, *it is desirable to scan* $\sin\theta$ *separately in the resonant and non-resonant regime.*

Scans of the $\sin\theta$ parameter show they have minimal effect on the kinematic distri-

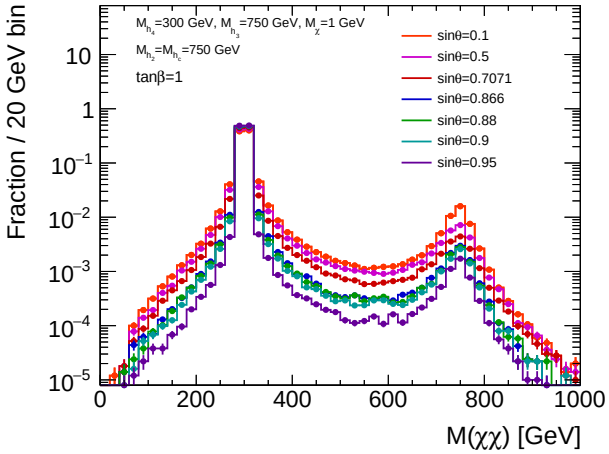

Figure 10: The mass distribution of the $\chi\bar{\chi}$ system for various values of $\sin\theta$, with $M_a = 300$ GeV, $M_A = 750$ GeV, $M_H = M_{H^\pm} = 750$ GeV, and $\tan\beta = 1$.

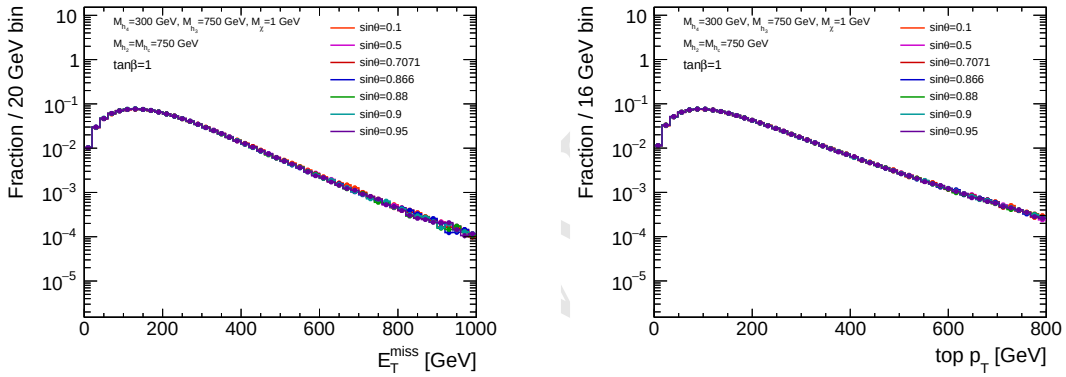

(a) E_T^{miss} (b) top p_T

Figure 11: The E_T^{miss} and top p_T distribution for inclusive $t\bar{t} + \chi\bar{\chi}$ production for various values of $\sin\theta$, with $M_a = 300$ GeV, $M_A = 750$ GeV, $M_H = M_{H^\pm} = 750$ GeV, and $\tan\beta = 1$.

butions for searches with a Z boson (Figure 12b).

In the $t\bar{t} + E_T^{\text{miss}}$ signature, the A (h_3 in the figure) and a (h_4 in the figure) mass peaks are quite narrow for values where $\sin\theta$ approaches 1, and $a \to \chi\bar{\chi}$ is the dominant $\chi\bar{\chi}$ production mode, as shown in Figure 10. However, no significant kinematic dependence on $\sin\theta$ is observed in the E_T^{miss} and top quark p_T as shown in Figure 11 before any analysis cuts are applied.

1.2.3 Ratio of the doublet vacuum expectation values ($\tan\beta$)

The shape of E_T^{miss} distribution also has a non-trivial dependence on $\tan\beta$, as can be seen in Figure 13. As discussed in the sensitivity study later, at small $\tan\beta$, the Yukawa coupling to top quark is large and the signal production mode is dominated by the non-resonant 3-body

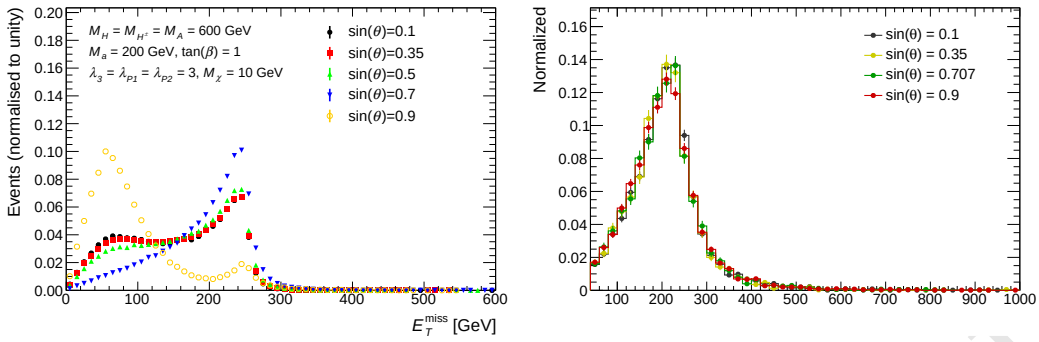

(a) E_T^{miss} distribution for for five representative models with different $\sin\theta$ and fixed $M_A = M_H = M_{H^\pm} = 600$ GeV, $M_a = 200$ GeV.

(b) E_T^{miss} distribution after preselection for scans of $\sin\theta$ for fixed $M_A = M_H = M_{H^\pm} = M_a = 250$.

Figure 12: E_T^{miss} distributions in $h(bb)+E_T^{\text{miss}}$ and Z(lep)+E_T^{miss} events for different $\sin\theta$. In both cases, $\tan\beta = 1$ and $M_\chi = 10$ GeV.

processes $gg \to h\chi\bar{\chi}$, which gives a broad and soft E_T^{miss} spectrum. As $\tan\beta$ increases, the contribution of resonant production increases as well and the Jacobian peak also appears. When the pseudoscalar A is produced off-shell, i.e. when $M_A < M_a + M_h$, the shapes of E_T^{miss} distributions become similar and the dependence on $\tan\beta$ disappears. For small values of $\tan\beta$ there is a slight softening and broadening of the E_T^{miss} distribution caused by the increased contribution from non-resonant $Z + a$ production in Z+E_T^{miss} searches.

In the $t\bar{t}$ + E_T^{miss} signature, and in the limit of small $\tan\beta$ values, the couplings of A (h_3 in the figure) and a (h_4 in the figure) to down-type quarks are heavily suppressed regardless of the Yukawa assignment. At LO, $t\bar{t} + \chi\bar{\chi}$ associated production is mediated through either CP-odd weak eigenstate, A or a, though it is shown in Figure 15 that $a \to \chi\bar{\chi}$ is the dominant production mode. Although the relative mediator contribution is dependent on $\tan\beta$, observables such as E_T^{miss} and top quark p_T only have a moderate kinematic dependence on $\tan\beta$ as demonstrated in Figure 16 before any analysis cuts. Other variables, such as the transverse mass M_T, are more affected by the contribution of the high mass mediator, as shown in Figure 16 after kinematic cuts. For this reason, and since the production cross section times branching ratio for the $b\bar{b}$ + E_T^{miss} signature is enhanced at high values of $\tan\beta$ (**Show cross-section plot when available**) *it is desirable to perform a coarse scan in* $\tan\beta$ *as well.*

1.3 Comparison with existing pseudoscalar models and recasting of HF+E_T^{miss} search results

To date, simplified models of DM [7, 8] that add a single scalar or pseudoscalar mediator and the DM particle to the SM are used as benchmarks for the Run II CMS and ATLAS HF+E_T^{miss} searches. These are called `DMsimp` models in the following. The kinematics and cross-section of the pseudoscalar `DMsimp` models can map directly onto those of the 2HDM+a model, when accounting for the contributions from the light and heavy

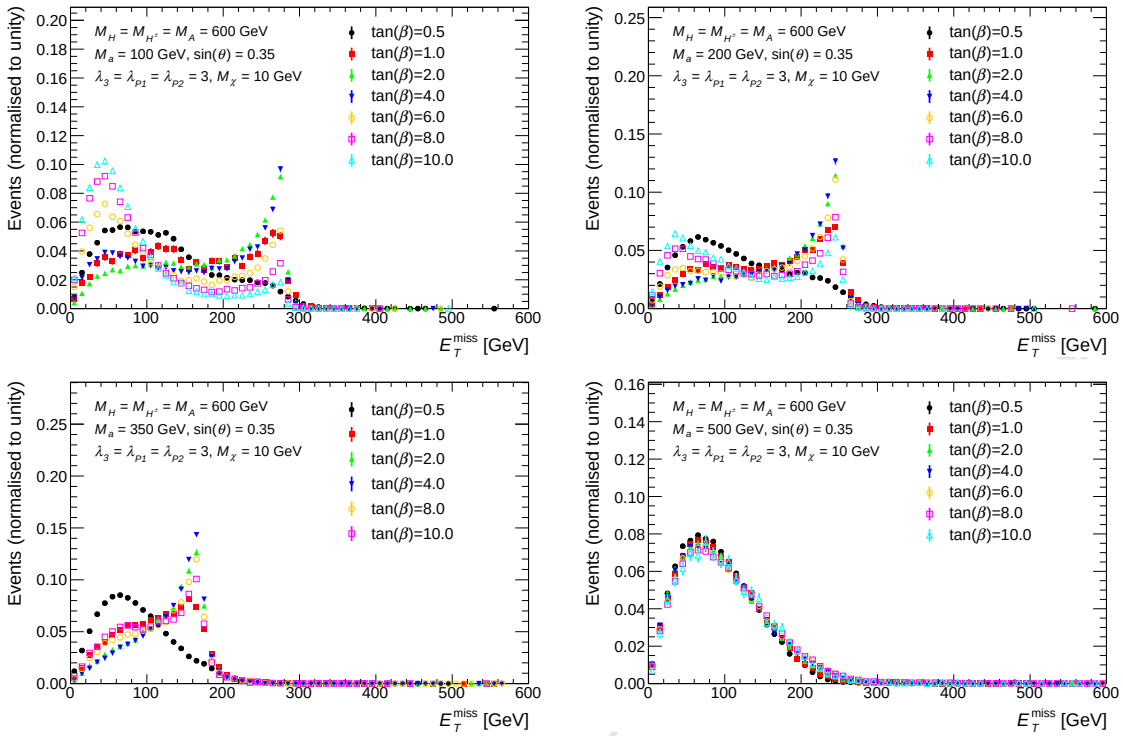

Figure 13: Missing transverse momentum distribution of $h \to bb + E_T^{\text{miss}}$ signal events at parton level with different $\tan\beta$ and fixed $M_A = M_H = M_{H^\pm} = 600$ GeV, $M_\chi = 10$ GeV, $\sin\theta = 0.35$, and $\lambda_{P1} = \lambda_{P2} = \lambda_3 = 3$. The values of M_a are set to 100, 200, 350, and 500 GeV, respectively. The shapes of the E_T^{miss} distributions for different $\tan\beta$ are similar when $M_A < M_h + M_a$. Note, in these figures, both the contributions of gg and $b\bar{b}$ initiated processes are included and a combined histogram is produced according to their corresponding cross sections.

pseudoscalar mediators.

The comparison of some of the relevant kinematic distributions between the pseudoscalar simplified model and the 2HDM+a model using two different values of M_a, is shown in Figure 18. In these figures, the parameters used are: $M_A = 600$ GeV, $M_H = M_{H^\pm} = 600$ GeV, $\sin\theta = 0.7071$, $\tan\beta = 1$, while M_a is either 100 or 600 GeV. The distributions for the two models agree when the mediator mass in the `DMsimp` model is set to M_a and the contribution from A decays is smaller since A is more massive than a.

The `DMSimp` model has only one mediator particle. Figure 19 shows that the 2HDM+a model can be represented as the sum of two contributions, one from the light pseudoscalar and the other one from the heavy pseudoscalar. This is because the HF+E_T^{miss} signatures are dominantly produced in diagrams involving the invisible decays of the two CP-odd scalars. The 2HDM+a model is equivalent to the single pseudoscalar simplified model `DMsimp` when A is much heavier than a, and therefore the former does not contribute to the considered final state. However, when the two mediators are closer in mass, the $pp \to ttA$ contribution becomes more relevant. This can be seen in Figure 20, where the

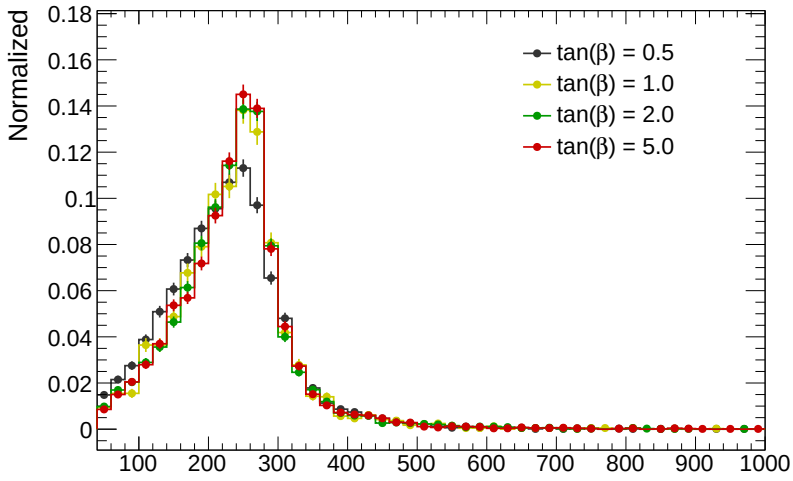

Figure 14: E_T^{miss} distribution after preselection for scans of $\tan\beta$ for fixed M_A =600 GeV and $M_a = 150$ GeV. This parameter has little impact on the kinematic distributions, except for small values of $\tan\beta$ where there is a slight softening and broadening of the E_T^{miss} distribution caused by the increased contribution from the top box feynman diagram.

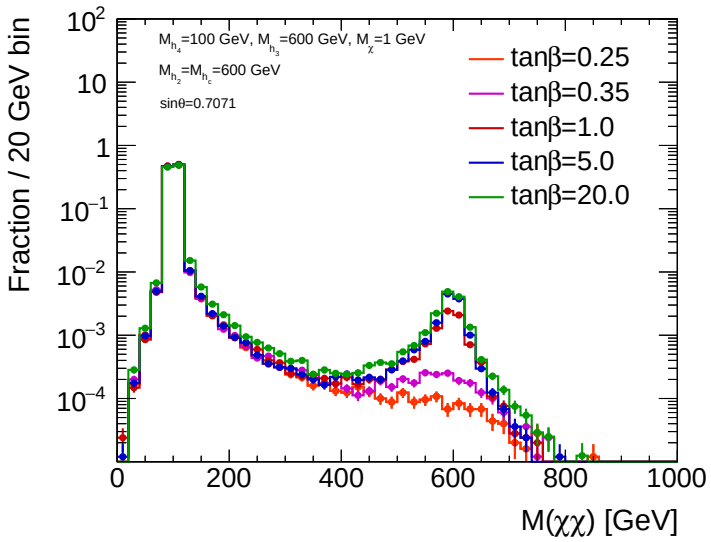

Figure 15: The mass distribution of the $\chi\bar{\chi}$ system for various values of $\tan\beta$, with $M_a = 100$ GeV, $M_A = 600$ GeV, $M_H = M_{H^\pm} = 600$ GeV, and $\sin\theta = 0.7071$.

two models are compared assuming $m(A) = 750$ GeV and two different values for $m(a)$. An excellent agreement is observed between `DMsimp` and 2HDM+a at parton-level variables sensitive to the helicity structure of the interaction between top and the mediator[9], if the invariant mass of the two DM particles in the 2HDM is smaller than 200(300) GeV for $m(a) = 150(300)$ GeV respectively. This gives confidence that, once the contribution

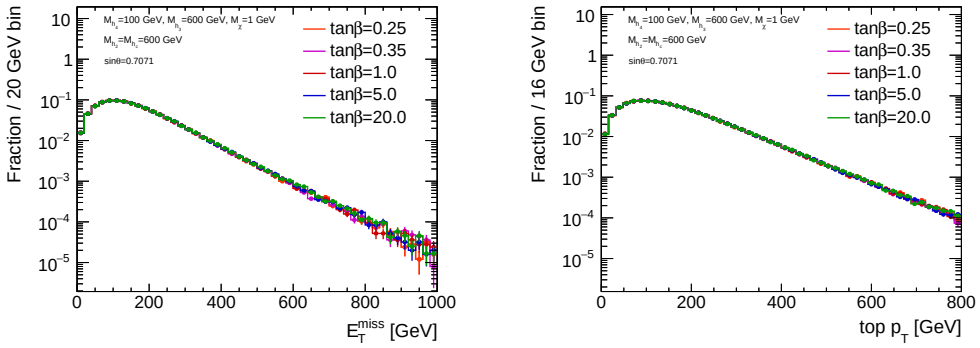

(a) E_T^{miss} (b) top p_T

Figure 16: The E_T^{miss} and top p_T distribution for inclusive $t\bar{t}+\chi\bar{\chi}$ production for various values of $\tan\beta$, with $\mathrm{M_a}$ = 100 GeV, $\mathrm{M_A}$ = 600 GeV, $\mathrm{M_H}$ = $\mathrm{M_{H^\pm}}$ = 600 GeV, and $\sin\theta = 0.7071$.

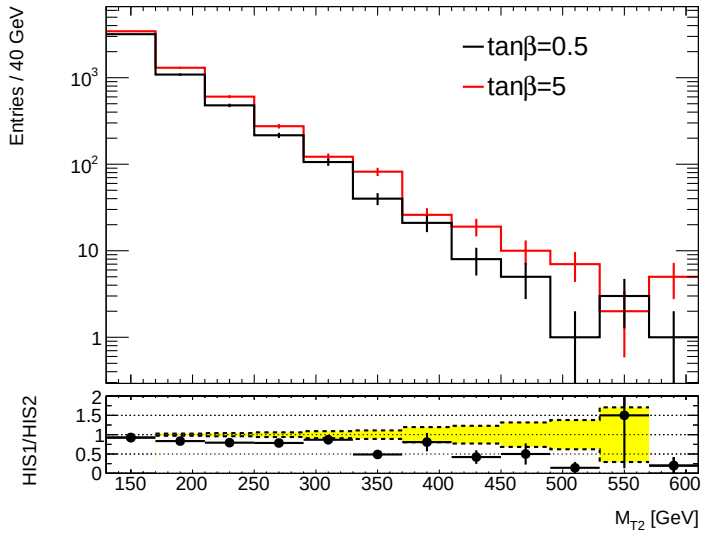

Figure 17: The M_T distribution in the $t\bar{t}$ + E_T^{miss} signature for different values of $\tan\beta$, after all selection cuts.

from A production is identified and separated, it is possible to fully map the $2HDM + a$ kinematics to the existing `DMsimp` model.

The mapping that can be used to reinterpret existing searches that use the `DMSimp` model is achieved by taking, for each set of the parameters, the average of the selection acceptances for $m(A)$ and $M(A)$ obtained from the `DMSimp` model, weighted by the respective cross-section for A (σ_A) and a (σ_a) production:

$$Acc_{2HDM}(m(A), M(a)) = \frac{\sigma_a \times Acc_{DMSimp}(m(a)) + \sigma_A \times Acc_{DMSimp}(m(A))}{\sigma_a + \sigma_A} \qquad (1.2)$$

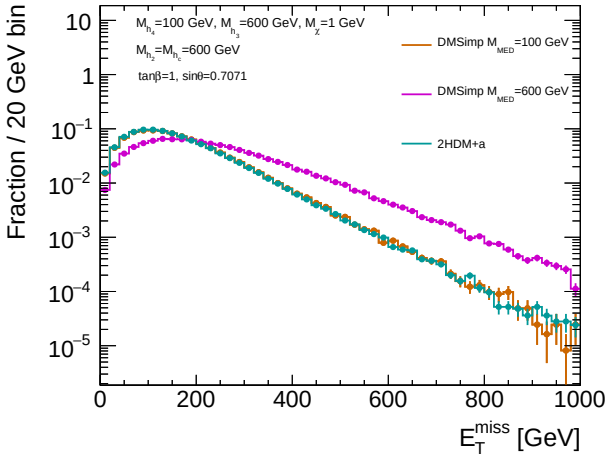

(a) E_T^{miss}

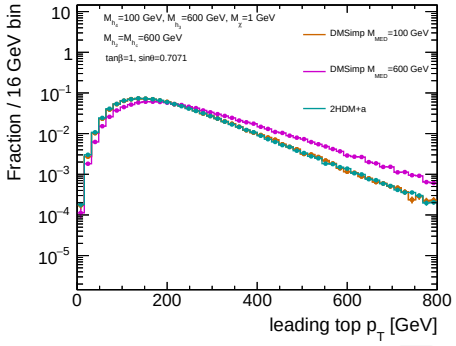

(b) Leading top p_T

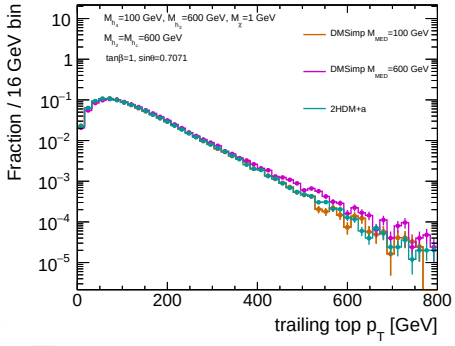

(c) Trailing top p_T

Figure 18: The E_T^{miss}, leading and trailing top p_T distributions for inclusive $t\bar{t} + \chi\bar{\chi}$ production for different values of M_a, with $M_A = M_H = M_{H^\pm} = 600$ GeV, $\tan\beta = 1$, M_χ =1 GeV and $\sin\theta = 0.7071$, compared to the `DMsimp` pseudoscalar model.

The acceptance in this case is obtained as a parton-level implementation of the two-lepton analysis described in [arXiv:1710.11412]. The acceptance estimated in this way is shown as red triangles in Figure 21, and an excellent agreement can be seen with the acceptances evaluated directly on the 2HDM samples. Further validation was performed also on the acceptances calculated as a function of $sin\theta$ and $tan\beta$. Finally, the formula was successfully tested also with $|M_A - M_a| \sim 50$ GeV, where interference between the production of the two bosons is possible.

2 Parameter grid

The studies in the previous section show that varying most of the model parameters lead to non-trivial modifications of the for the H+E_T^{miss} and Z+E_T^{miss} searches. The benchmark model points that have been agreed within the DMWG and are suggested here do not provide an exhaustive scan the entire parameter space of this model, but highlights many

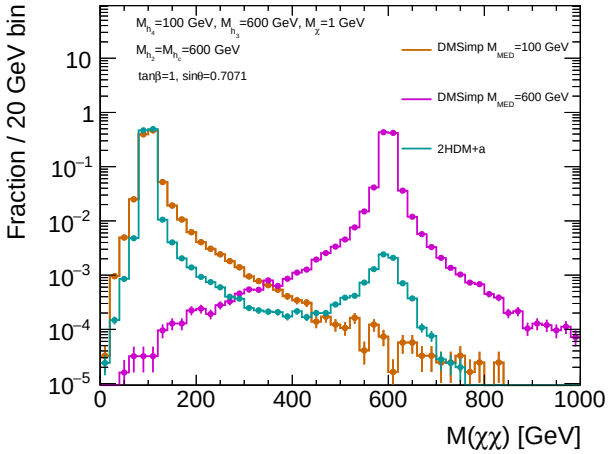

Figure 19: The mass distribution of the $\chi\bar{\chi}$ system for `DMsimp` pseudoscalar models with M_a = 100 GeV and M_a = 600 GeV, compared with 2HDM+a with M_a = 100 GeV, M_A = 600 GeV, $M_H = M_{H^\pm}$ = 600 GeV, $\sin\theta = 0.7071$ and $\tan\beta = 1$. TODO: needs different markers.

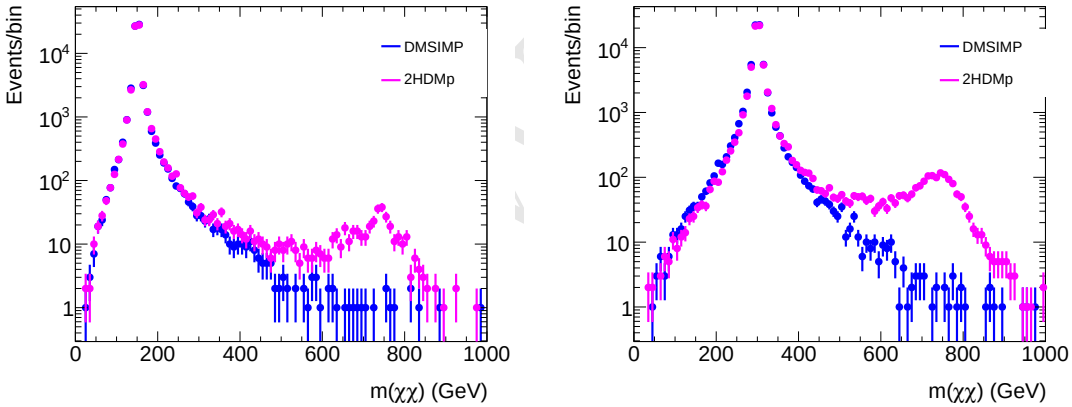

Figure 20: Comparison of $m(\chi\chi)$, the invariant mass of the two DM particles for the `DMSimp` (blue) and the $2HDMp$ model (magenta) with $m(A) = M_{med}$ = 750 GeV. The plot on the left uses M_a =150 GeV, while the plot on the right uses M_a =300 GeV.

of the features that are unique of this model and the complementarity of the various signatures.

Scan in the M_a, $M_A = M_H = M_{H^\pm}$ plane The main parameter grid proposed to investigate this model with LHC data spans combinations of the light pseudoscalar mass (M_a) and the heavy pseudoscalar mass (M_A) plane, fixing $M_A = M_H = M_{H^\pm}$. The mixing angle $\sin\theta$ is fixed to 0.35, to evade precision constraints. $\tan\beta$ is fixed to unity to obtain a mixture of resonant and non-resonant processes for the H+E_T^{miss} and Z+E_T^{miss} searches.

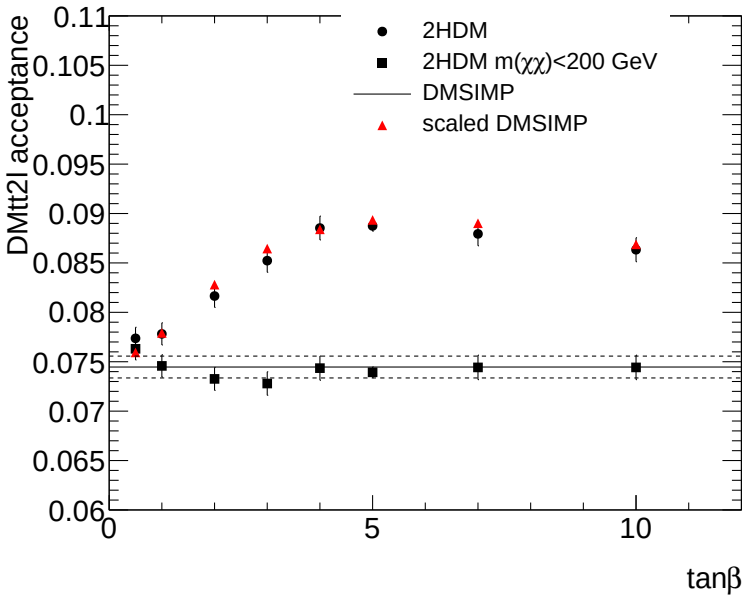

Figure 21: Acceptance of the two-lepton analysis as a function of $\tan\beta$ for the $2HDMp$ model (round markers), for the $2HDMp$ model considering only events with $m(\chi\chi) <$ 200 GeV (square markers), and for the `DMSimp` model (full line) for a mediator mass of 150 GeV. The two dashed lines indicate the statistical error of the `DMSimp`. The value of $m(A)$ is fixed at 600 GeV, and $\sin\theta = 0.35$. The acceptance calculated from the `DMSimp` acceptance rescaled following the prescription in Equation 1.2 (red triangles) is also shown.

The DM particle mass is fixed to 10 GeV, to obtain cross-sections that are sufficiently large to be probed by Run-2 LHC searches. The spacing of the grid in M_a and M_A is left to the individual searches. The parameters $\sin\theta$, $\tan\beta$ and M_χ are scanned separately.

Scan in the M_a, $\tan\beta$ plane A two-dimensional scan in the M_a, $\tan\beta$ plane, fixing $M_A = M_H = M_{H^\pm} = 600$ GeV, is used to emphasize the complementarity of the H+E_T^{miss} and Z+E_T^{miss} searches with the heavy flavor + E_T^{miss} searches. The scan in M_a includes masses between 10 and 350 GeV, while the $\tan\beta$ scan includes $\tan\beta$ = 50, 45, 40, 35, 30, 25, 20, 15, 10, 5, where the high-$\tan\beta$ points are of primary interest for the heavy flavor searches.

Scans in sin_θ Two one-dimensional scans in sin_θ are also suggested for further comparison of the H/Z+E_T^{miss} and $b\bar{b}$+E_T^{miss} analyses. In the first scan, resonant processes dominate with $M_A = M_H = M_{H^\pm} = 600$ GeV and M_a =200 GeV, while in the second scan $M_A = M_H = M_{H^\pm} = 1000$ GeV and M_a =350 GeV. For both scans, $\tan\beta$ and the DM mass are fixed to $\tan\beta$=1 and $M_\chi = 10$ GeV.

Scan in M_χ A one-dimensional scan in M_χ spanning from 1 GeV to 500 GeV, with fixed M_A =M_H =600 and M_a =250 GeV, is also suggested to connect this model to a standard cosmological history. Even though the model points with where the DM particle has a

mass above 100 GeV are not within immediate reach of Run-2 searches, the measured relic density is satisfied by this model at values of DM mass around 100 GeV, as shown in **??**.

References

[1] **ATLAS** Collaboration, M. Aaboud et al., *Search for Dark Matter Produced in Association with a Higgs Boson Decaying to $b\bar{b}$ using 36 fb^{-1} of pp collisions at $\sqrt{s} = 13$ TeV with the ATLAS Detector*, arXiv:1707.01302.

[2] L. M. Carpenter, A. Nelson, C. Shimmin, T. M. Tait, and D. Whiteson, *Collider searches for dark matter in events with a Z boson and missing energy*, arXiv:1212.3352.

[3] N. F. Bell, J. B. Dent, A. J. Galea, T. D. Jacques, L. M. Krauss, et al., *Searching for dark matter at the LHC with a mono-Z*, *Phys.Rev.* **D86** (2012) 096011, [arXiv:1209.0231].

[4] **ATLAS** Collaboration, M. Aaboud et al., *Search for an invisibly decaying Higgs boson or dark matter candidates produced in association with a Z boson in pp collisions at $\sqrt{s} = 13$ TeV with the ATLAS detector*, *Phys. Lett.* **B776** (2018) 318–337, [arXiv:1708.09624].

[5] **CMS** Collaboration, A. M. Sirunyan et al., *Search for new physics in events with a leptonically decaying Z boson and a large transverse momentum imbalance in proton-proton collisions at $\sqrt{s} = 13$ TeV*, arXiv:1711.00431.

[6] M. Bauer, U. Haisch, and F. Kahlhoefer, *Simplified dark matter models with two Higgs doublets: I. Pseudoscalar mediators*, *JHEP* **05** (2017) 138, [arXiv:1701.07427].

[7] D. Abercrombie et al., *Dark Matter Benchmark Models for Early LHC Run-2 Searches: Report of the ATLAS/CMS Dark Matter Forum*, arXiv:1507.00966.

[8] M. Backovic, M. Krämer, F. Maltoni, A. Martini, K. Mawatari, and M. Pellen, *Higher-order QCD predictions for dark matter production at the LHC in simplified models with s-channel mediators*, *Eur. Phys. J.* **C75** (2015), no. 10 482, [arXiv:1508.05327].

[9] U. Haisch, P. Pani, and G. Polesello, *Determining the CP nature of spin-0 mediators in associated production of dark matter and $t\bar{t}$ pairs*, arXiv:1611.09841.